Improving Power Response of Single-controllable VSG-based Active Distribution Network

Shah Fahad, Arman Goudarzi, Pierluigi Siano, and Ji Xiang, *Senior Member*, *IEEE*

***Abstract*—Controlling an active distribution network (ADN) from a single PCC has been advantageous for improving the performance of coordinated Intermittent RESs (IRESs). Recent studies have proposed a constant PQ regulation approach at the PCC of ADNs using coordination of non-MPPT based DGs. However, due to the intermittent nature of DGs coupled with PCC through uni-directional broadcast communication, the PCC becomes vulnerable to transient issues. To address this challenge, this study first presents a detailed mathematical model of an ADN from the perspective of PCC regulation to realize rigidness of PCC against transients. Second, an H_∞ controller is formulated and employed to achieve optimal performance against disturbances, consequently, ensuring the least oscillations during transients at PCC. Third, an eigenvalue analysis is presented to analyze convergence speed limitations of the newly derived system model. Last, simulation results show the proposed method offers superior performance as compared to the state-of-the-art methods.**

***Index Terms*—Cooperative control of DGs, hierarchical control system, high penetration of intermittent RESs, H_∞ control, optimal control in power systems, single-controllable active distribution networks.**

I. Introduction

INTEGRATION of intermittent renewable energy sources (IRESs) into passive distribution networks have led transition towards active distribution networks (ADNs) [1]. However, this transition has brought forth new challenges that include voltage rise (due to reverse power flow), unconsumed excess power from IRESs operated in maximum power point tracking (MPPT) mode, and power fluctuations due to the intermittent nature of wind turbine generators (WTGs) and photovoltaic generators (PVGs).

Existing ADNs are being energized by a small percentage of IRESs while the rest of the demand is being fed by other sources which mostly rely on synchronous generators (SGs). Currently, IRESs are operated with MPPT modes which compel the source to inject all available energy to the grid without taking notice of the load demand. Since, penetration of IRESs compared to SGs based generation is low, therefore, injecting all the available energy into the grid is economically feasible. However, when penetration of IRESs is high as compared to the SGs based generation, only the economical perspective might not suffice. For instance, consider an ADN where high penetration of MPPT-enabled IRESs are injecting all available energy to the grid without considering the load demand. During the event when the load demand is less than generation, excess power will create an imbalance of power which will inflict severe consequences for the grid such as frequency deviation, voltage rise, and power dispatch issues [2].

These problems can significantly be overcome by operating the IRESs without MPPT controller device. Moreover, if active and reactive power (PQ) at the point of common coupling (PCC) of an ADN is regulated to a constant value, then the whole ADN will exhibit features of a PQ node thus making it a single-controllable ADN [3]. In other words, the PCC can be manipulated to inject only the desired amount of active and reactive power from the ADN to the grid thus saving the grid from overwhelming power. Furthermore, the active and reactive powers of the non-MPPT operated IRESs can be coordinated in such a manner that the PCC of ADN is regulated as a constant PQ node [2].

To regulate the PCC as a constant PQ node, a broadcast communication is required between local nodes of DGs and high voltage PCC. Moreover, DGs require bi-directional communication to establish coordination among them. Therefore, the response of DGs is directly coupled with active and reactive power of PCC, consequently, creating various complications. For instance, any change in load, irradiance (for PVGs), or wind speed (for WTGs) will vary output power from DGs. Varying load, and output power variation from DGs directly inflicts undesired fluctuations in the PQ demand management at PCC of ADN.

A. Literature Review

In this regard, several studies have proposed coordination control strategies to subdue the affect of IRESs on the PCC of ADN.

The authors in [4] presented a coordination control strategy for load management and voltage regulation using battery energy storage system (BESS). However in this method, the loss

Manuscript received October 28, 2022; revised January 6, 2023; accepted May 31, 2023. Date of online publication September 8, 2023; date of current version October 30, 2024. This work is supported by the National Natural Science Foundation of China (No: 62173295).

S. Fahad (corresponding author, email: shah.fahad072@gmail.com) is with the Department of Electrical and Computer Engineering, Missouri University of Science and Technology, USA.

A. Goudarzi is with the University of Victoria, Canada.

P. Siano is with the Department of Management & Innovation Systems, University of Salerno, Italy; and also with the Department of Electrical and Electronic Engineering Science, University of Johannesburg, Johannesburg 2006, South Africa.

J. Xiang is with the National Laboratory of Industrial Control Technology, and the College of Electrical Engineering, Zhejiang University, Hangzhou 310058, China.

DOI: 10.17775/CSEEJPES.2022.07380

of leader can cause complete shut down of the whole system. In [5], a new method for energy management of various DGs is considered; nevertheless, the PQ regulation feature at PCC of ADN is neglected. Moreover, studies in [6], [7] proposed energy management strategies for distantly located energy sources to suppress influence of intermittency of IRESs on the grid. The authors in [8] proposed an energy management scheme for multiple PVGs in order to inject constant power to the grid. In [9], a study based on constant power injection to the grid through using coordinated tuning of WTGs and BESS is proposed. These studies have applied constant PQ management at PCC of ADN while suppressing intermittency of IRESs through utilizing BESS. However, coordination among IRESs is not considered. Whereas, the proposed strategy focuses on coordination among IRESs. Authors in [10] reported a method to suppress fluctuations at tie-line using the BESS and demand response program. Nonetheless, this method relies on a centralized architecture. Failure of the central computer can sabotage the whole operation [11]. A power management strategy at PCC along with addition of power quality enhancement feature is presented in [12]. However, this method requires a converter directly attached to the PCC. Few studies have proposed distributed control techniques for parallel operation of DGs. For instance, the authors in [13] proposed a distributed control scheme to optimize active power output from parallel operating IRESs. Similarly, a consensus based distributed control strategy is presented in [14], where power management among IRESs is achieved in a coordinated manner. In addition, the authors in [15] proposed an energy management scheme to optimize the active power dispatch from parallel operating IRESs. Moreover, an optimized resource allocation scheme using multi-agent framework is presented in [16]. Furthermore, in [17], a consensus based distributed control algorithm is proposed to optimize power dispatch among DGs considering local estimation of power mismatch. However, these distributed control methods only consider active power management. Ignoring reactive power management can have serious consequences with voltages in the system.

In this context, both active and reactive power management is considered in [18] and [19]. However, the only drawback is that these methods use derivative for terminal voltage that could magnify noise components and lead to power quality degradation.

Some rare methods also proposed coordination of virtual synchronous generator (VSG) controlled DGs. The authors in [20] proposed a master-slave configuration for VSGs. In this strategy, VSGs operate at MPPT during steady-state mode while in transient mode operation is transitioned to $P-\omega$ mode. In [21], the authors presented a coordination scheme for VSGs which uses adaptive values of the moment of inertia (J) and damping (D) to suppress power oscillations during disturbances. In a different context, the authors in [22] proposed a decentralized method to handle power management among several sources. However, these studies are mainly focused on coordination of IRESs in an autonomous system without considering the single-controllable feature of ADN.

Furthermore, another VSG-based power management strategy is presented in [23]; nevertheless, coordination among IRESs is ignored. Until this point, the above literature either proposed coordination of IRESs or PQ regulation at PCC whereas the proposed study aims to implement both simultaneously. In this regard, the strategy presented in [2] uses coordination of grid feeding converters to achieve PQ regulation at PCC of ADN. Nevertheless, the use of grid feeding converters inflict severe oscillations on the PCC of ADN whereas disproportionate reactive power used to achieve voltage balance may lead to circulating reactive power issues as shown in [3].

Aiming to curb drawbacks of the above studies, a unique method was presented by [3] and [24] to share active and reactive powers of VSG controlled DGs proportionately in order to achieve common power factor, as well as constant PQ demand management at the PCC of ADN. As per the requirement of application, this method serves well. However, the aforementioned studies ([3]) and [24]) did not consider mathematical modeling and quantitative analysis of rigidness of the PCC of ADN. Moreover, regulating the PCC as a constant PQ node can inflict severe consequences for the PCC itself. For instance, active and reactive power controllers at PCC are directly linked with generation of IRESs through unidirectional broadcast communication. Moreover, until consensus is reached, bi-directional communication-based distributed control among DGs keep changing the active and reactive power output from DGs. Any change in active and reactive power output of DGs will induce error in the controller of the PCC. For this reason, dynamics of IRESs influence rigidness of the PCC of ADN. More importantly, mathematical models proposed in the above literature review are given in isolated form. For instance, the primary control layer in [3], [24] holds the swing equation for VSG, while in [2], the primary control layer is based on grid feeding converter control law. Whereas, the tertiary control layer models hold proportionate active and reactive power in [3], [24] and active power sharing with voltage balancing feature in [2]. The above mentioned strategies lack modeling of influence of dynamics of one control layer over the other. Therefore, the influence of dynamic elements from coordinated DGs on the PCC regulation can not be analyzed. The proposed study expands the existing study by proposing a simple but an essential model that mathematically represents the influence of dynamic elements of primary and tertiary control layer over the secondary control layer. In addition, the proposed study proposes representation of rigidness of PCC as H_∞-norm which was made possible using the proposed mathematical model. To categorically highlight contributions of the proposed study, the above literature review is presented in Table I.

Owing to the aforementioned deficiencies, the proposed study aims to improve the previously presented method in [3] by not only introducing a detailed mathematical model that contains dynamics of coordination of IRESs, but also, to reduce implications of dynamics from IRESs on rigidness of the PCC. In this study, a comprehensive mathematical model is presented to realize the nature of the PCC in terms of how rigid it is against disturbances. Moreover, an H_∞ sub-optimal

TABLE I
COMPARISON OF THE PROPOSED STUDY WITH THE STATE-OF-THE-ART METHODS.

References	Regulating PCC	DGs Coordination	Power Factor Improvement	Dynamic Model Representation	PCC Rigidness Optimization
[25]–[28]	✓	✗	✗	✗	✗
[5], [20]–[22]	✗	✓	✗	✗	✗
[6]–[9], [23]	✓	✗	✗	✗	✗
[12]	✓	✗	✓	✗	✗
[10]	✓	✗	✗	✗	✗
[13]–[19], [24]	✓	✓	✗	✗	✗
[2]	✓	✓	✗	✗	✗
[3]	✓	✓	✓	✗	✗
The proposed strategy	✓	✓	✓	✓	✓

controller is derived that successfully enhances rigidness of the parameters at PCC by reducing the H_∞ norm of the closed loop system. Furthermore, the convergence speed of the proposed model is assessed to avoid an undesired/slow response of the model.

The main contributions of the proposed study are:

- A complete mathematical formulation of the aggregated plant model is derived that includes dynamics of parallel operating converters and their effect on active and reactive power of PCC. Contrary to [2], [3], [24], the proposed method mathematically represents the relation between dynamics of primary control layer and tertiary control layer on the PQ management of the PCC of ADN. It is shown that, the proposed model provides the opportunity to evaluate the nature of the rigidness of PCC.
- Motivated to enhance rigidness of parameters at PCC, an H_∞ controller is derived to minimize closed-loop gain of the PCC. With this approach, it becomes possible to optimize the response of PQ parameters at the PCC.
- Eigenvalue analysis of the proposed model is also presented to evaluate limits of the convergence speed of the proposed model. Moreover, the proposed method is validated on a generic IEEE 13-bus and IEEE 34-bus test system.

The benefits of the proposed method over conventional methods can be highlighted as:

- Optimized active and reactive power regulation rigidness at PCC which improves dynamics at PCC.
- Suppressing overshooting peaks at PCC keeps substation transformer and power electronics converters from overloading.
- Improving dynamics of active and reactive power management at PCC have also led to the improvement in performance of frequency of the system as well.

II. PRELIMINARIES

The proposed study is mainly focused on the modification of secondary controller; however, the role of primary and tertiary control layer cannot be ignored. For the purpose of clarity, a brief introduction of the role of primary and tertiary control layer is presented in subsections below. Moreover, a brief discussion on influence of system dynamics on the PCC regulation is also presented.

A. Primary Control Layer

As shown in Fig. 1, each DG in the ADN is equipped with VSG control which is operated without MPPT mode. With VSG control, DGs emulate the behavior of a SG, thereby, enhancing the inertial response of the system. The electro-mechanical equation used in the proposed system is expressed as:

$$J_{\rm vsg}\omega_{\rm vsg}\frac{{\rm d}\omega_{\rm vsg}}{{\rm d}t} = P_{\rm vsg} - P_e - D(\omega_{\rm vsg} - \omega_n) \tag{1}$$

here, $J_{\rm vsg}$, $\omega_{\rm vsg}$ and ω_n is moment of inertia, angular frequency of virtual shaft and nominal angular frequency, respectively; $P_{\rm vsg}(or P_{\rm ref})$, and P_e, represents virtual mechanical power and electrical power, respectively; virtual damping is represented by D.

Reactive power regulation in the proposed method is expressed as:

$$K_{\rm inertia}\frac{{\rm d}E^d_{\rm ref}}{{\rm d}t} = (Q_{\rm ref} - Q_{\rm vsg}) + K_q(|V_g| - V^d_{\rm vsg}) \tag{2}$$

here, $K_{\rm inertia}$ is the virtual inertia constant of excitation controller and $E^d_{\rm ref}$ is the reference voltage for converter output.

Due to on-going replacement of SGs with MPPT mode DGs, the inertia constant of the overall power systems is declining. With loss of heavy rotating rotor, which is the key inertia element in power systems, primary control based on governor response is lost due to which the system experiences high RoCoF along with taking less time to reach frequency nadir. Therefore, the proposed study uses VSG control based primary control layer for all DGs in a coordination cluster to retain the declining inertia constant. Depending on the control strategy adopted for the DGs, the overall inertia (including the virtual inertial) constant of the power system can be expressed by [30]:

$$H_{\rm sys} = \sum_{i=1}^{n_s} H_{{\rm SG}i} * \frac{S_{{\rm G}i}}{S_{\rm sys}} + \sum_{i=1}^{n_d} H_{{\rm DG}i} * \frac{S_{{\rm DG}i}}{S_{\rm sys}} + \sum_{i=1}^{n_d} H_{{\rm BESS}i} * \frac{S_{{\rm BESS}i}}{S_{\rm sys}} \tag{3}$$

here, subscripts $S_{{\rm G}i}$, $S_{{\rm DG}i}$, $S_{{\rm BESS}i}$ notes the apparent power of the $i^{\rm th}$ SG, DG, and BESS, respectively; terms $H_{{\rm SG}i}$, $H_{{\rm DG}i}$, $H_{{\rm BESS}i}$ represent inertia constant of SG and virtual inertia constant for DGs and BESS. It is pertinent to mention

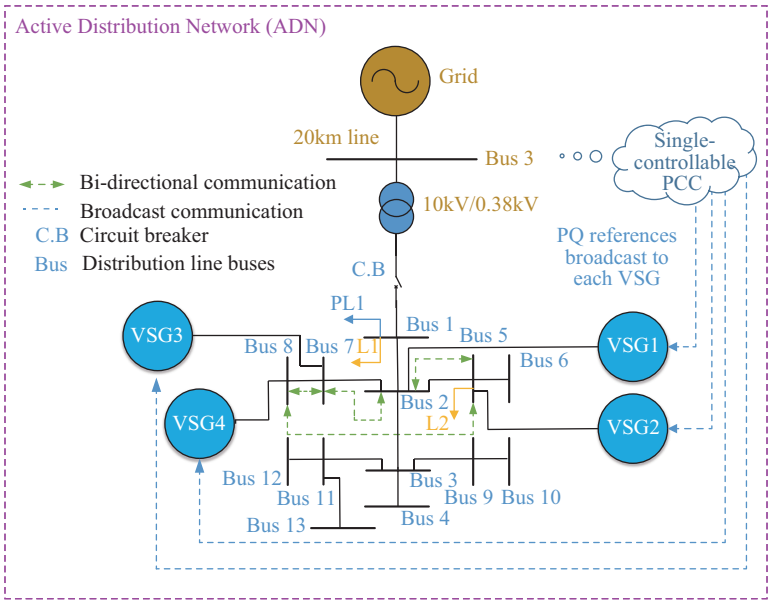

Fig. 1. Controller validation using the IEEE 13-bus distribution distribution system [29].

that, the proposed study uses coordination of a cluster of VSG controlled DGs to regulate the PCC of ADN as a constant PQ node. In this manner, the whole cluster of DGs (with non-MPPT operation) responds to requirements of the PCC in a coordinated manner thus improving the performance of frequency of the overall ADN. In addition, the use of non-MPPT operation implies that the DGs will generate less power than its maximum capacity until the consensus index is less than 1. The consensus index will be discussed under the tertiary control layer subsection. The consensus index, if less than 1, ensures reserve power will generally be available which can be used to overcome disturbances. The reserve power can be expressed as:

$$P_{\mathrm{dg}} = P_{\mathrm{ava}} - \Delta P \tag{4}$$

here, P_{dg} and P_{ava} are generated output power and available power, respectively; and ΔP corresponds to reserve power available for power dispatch during disturbances.

In primary control hierarchy, each VSG receives active and reactive power references dispatched from secondary and tertiary control layers (to be discussed in the next subsection) as:

$$P_{\mathrm{ref}} = P_{\mathrm{isec\text{-}ref}} + P_{\mathrm{iTer\text{-}ref}} \tag{5}$$

$$Q_{\mathrm{ref}} = Q_{\mathrm{isec\text{-}ref}} + Q_{\mathrm{iTer\text{-}ref}} \tag{6}$$

B. Tertiary Control Layer

For this layer, parallel operating VSGs are equipped with a consensus-based distributed algorithm for bi-directional information exchange among them. For bi-directional communication, graph theory is used. Detailed information regarding the graph theory can be accessed at [31]. In the proposed strategy, each DG exchanges its active and reactive power information with its neighboring DG. The tertiary controller varies references in each iteration while keeping notice of the consensus index. Consensus indexes are $\alpha = \frac{P}{P^*}$ and $\beta = \frac{Q}{Q^*}$ for active and reactive power, respectively. Here, terms P^* and Q^* define available active and reactive power while terms P and Q denote output active and reactive power from each DG. The iteration process of formulating new references is carried out using the following expression

$$P_{\mathrm{iTer\text{-}ref}}(k+1) = P_i(k) + \rho \sum_{j=1}^{n} -l_{i,j}\alpha_j(k) \tag{7a}$$

$$Q_{\mathrm{iTer\text{-}ref}}(k+1) = Q_i(k) + \sigma \sum_{j=1}^{n} -l_{i,j}\beta_j(k) \tag{7b}$$

here, $P_i(k)$ and $Q_i(k)$ are active and reactive power of i^{th} VSG during previous iteration; term $P_{\mathrm{iTer\text{-}ref}}(k+1)$ and $Q_{\mathrm{iTer\text{-}ref}}(k+1)$ represent new active and reactive references; $l_{i,j}$ represents the weightage between neighbouring DGs; $\alpha_j(k)$ and $\beta_j(k)$ are active and reactive power consensus indexes. When α and β of all the DGs converge to a common value, the consensus is reached. At this point, if the consensus index converges to a value of 0.7, it means that all DGs are generating 70% of their respective available power.

C. Influence of System Disturbances on the PCC Regulation

In order to fulfill active and reactive power demand at PCC (bus 3 in Fig. 1), the following condition should be met:

$$P^*_{\mathrm{pcc}} = \sum_{j \epsilon S_E}^{n} P_{Gj} - \sum_{i \epsilon S_L}^{n} P_{Li} - P_{\mathrm{loss}} = P_{\mathrm{pcc}} \tag{8a}$$

$$Q^*_{\mathrm{pcc}} = \sum_{j \epsilon S_E}^{n} Q_{Gj} - \sum_{i \epsilon S_L}^{n} Q_{Li} - Q_{\mathrm{loss}} = Q_{\mathrm{pcc}} \tag{8b}$$

here, terms P^*_{pcc} and Q^*_{pcc} are active and reactive power demand at PCC; terms with subscript Gj represent generation of j^{th} DG; subscript L_i represents consumption of i^{th} load; P_{loss} and Q_{loss} are active and reactive power losses. If $P_{\mathrm{pcc}} = P^*_{\mathrm{pcc}}$ and $Q_{\mathrm{pcc}} = Q^*_{\mathrm{pcc}}$, it confirms that the demand of PCC has been fulfilled. Observing (8a) and (8b) shows that,

the satisfaction of $P_{\rm pcc} = P^*_{\rm pcc}$ and $Q_{\rm pcc} = Q^*_{\rm pcc}$ confirms that load as well as losses have been fulfilled. Therefore, specific information regarding load and losses in the system are not required.

From (8a) and (8b) it can be observed that, apart from losses, there are six apparent dynamic elements in the system which can influence the steady-state of the PCC. For instance, generation from DGs (P_{Gj}) and/or P_{Li}, if varied, term $P_{\rm pcc}$ will deviate from demand $P^*_{\rm pcc}$. This deviation will induce error in demand management at PCC. The amplitude of the induced error decides the intensity of rigidness at the PCC. For instance, if output power variation from IRESs inflicts high amplitude of error in demand management, the PCC is then termed as less rigid. If the designed controller can suppress oscillations in demand management, then rigidness of the PCC is enhanced. Moreover, it can be observed in Fig. 1 (bus 3 near the grid) that, the variations in parameters at PCC are directly influencing secondary terminals of the substation transformer. Power variation from high penetration of IRESs will cause huge oscillations at PCC which consequently can inflict high inrush currents and voltage oscillations. These disturbances can overwhelm secondary terminals of the transformer. Therefore, suppressing these oscillations is the main priority of the proposed study.

III. The Proposed h_∞ Control

A. Mathematical Model of the Plant

The main priority of the proposed control architecture is to fulfill active and reactive power demand at PCC of ADN with enhanced rigidness. For this reason, only secondary control of the proposed strategy is highlighted in detail. In order to satisfy (8a) and (8b), active and reactive power at PCC is regulated through a controller. The generated references are expressed as:

$$P_{\text{sec-ref}} = K_p(P^*_{\rm pcc} - P_{\rm pcc}), Q_{\text{sec-ref}} = K_q(Q^*_{\rm pcc} - Q_{\rm pcc}) \tag{9}$$

here, $P_{\text{sec-ref}}$ and $Q_{\text{sec-ref}}$ are generated references broadcast to each DG to satisfy the demand of the PCC. During the steady-state condition, i.e., when (8a) and (8b) are satisfied, then $P_{\text{sec-ref}}$ and $Q_{\text{sec-ref}}$ are equal to zero. Meanwhile, the proportionate active and reactive power sharing among DGs is handled by the tertiary control layer.

In the proposed study, an H_∞ controller is derived to enhance rigidness of parameters at PCC. The H_∞ control problem formulation is given in Figs. 2. References generated by the secondary control layer are broadcast to all DGs. Due to page restrictions, only derivation for active power is proposed; however, the same process is followed to derive the controller for reactive power demand. The active power signal received at each DG can be added to state equations of the DGs as:

$$\dot{P}_i = -P_i/\tau_i + P_{\text{sec-ref}}/\tau_i \tag{10}$$

here, τ_i represents the moment of virtual inertia of $i_{\rm th}$ VSG; and P_i is active power from $i_{\rm th}$ DG involved in the coordination cluster. The proposed model will use a network of four DGs, therefore i will be considered as $1-4$ for each

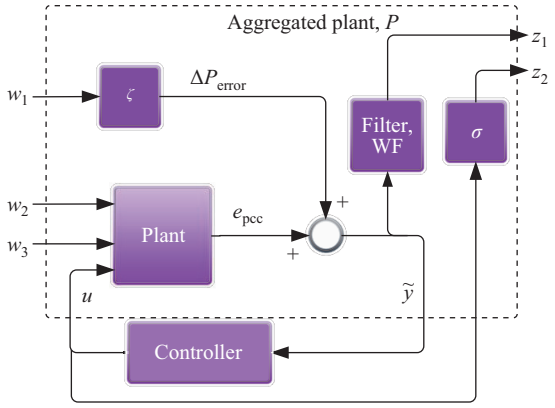

Fig. 2. H_∞ control problem.

DG. Since, the active power from DGs at the primary control layer follows the references dispatched from the secondary and tertiary control layers, therefore, dynamics of primary control of each DG are reflected in $P_1 - P_4$. During the steady-state, the term $P_1 - P_4$ is equivalent to $P_{\rm ref}$ given in (6). After a disturbance (either load variation, and/or, variation in output power from DGs), an error emerges at the PCC of ADN which creates an imbalance at (8a) and (8b). The demand and supply error, if not controlled in a timely manner, will influence voltage performance of the substation transformer. Moreover, this error is also coupled with DGs through the reference input signal which can further distort performance of DGs and could possibly lead them towards instability. This error is considered as an output regulating error which is fed to controller for regulation. The output equation or measured error at PCC is given by:

$$e_{\rm pcc} = P_{\rm pcc} - P^*_{\rm pcc} \tag{11}$$

From (8a), the power at PCC can be expressed as:

$$P_{\rm pcc} = P_L - P_1 - P_2 - P_3 - P_4 \tag{12}$$

here, for the sake of simplicity, losses are considered as part of load P_L. By inserting (12) in (11), the new output equation is written as:

$$e_{\rm pcc} = P_L - P_1 - P_2 - P_3 - P_4 - P^*_{\rm pcc} \tag{13}$$

here, $e_{\rm pcc}$ is the error between actual active power at PCC and the demand. The objective of the proposed controller is to minimize $e_{\rm pcc}$ to zero. Input (10) and output (13) state-space model of the proposed plant can be compared to generalized input and output state-space equations to extract the corresponding state, input, output and feed-forward matrices. The generalized state-space model can be expressed as:

$$\dot{x} = Ax + B_1 w + B_2 u \tag{14}$$

$$y = Cx + D_1 w + D_2 u \tag{15}$$

here, $\dot{x}$ is the input state equation equivalent to (10), and y is the output equation which is equated to $e_{\rm pcc}$ for the proposed application; u is the control signal which is equivalent to $P_{\text{sec-ref}}$ in our application; w is the exogenous input which, according to our plant, holds three separate exogenous inputs

such that $w = [w_1\ w_2\ w_3]^{\mathrm{T}}$ and can be represented by $w = [\Delta P_{\mathrm{error}}\ P_L\ P^*_{\mathrm{pcc}}]^{\mathrm{T}}$. Where, P_{error} is the error in the measured error signal, P_L is the load demand within the ADN, and P^*_{pcc} is the power demand at PCC. Each of the aforementioned parameters and their role in controlling the plant are illustrated in Figs. 2. By comparing (10) with (14), and, (13) with (15), the corresponding matrices of the system are derived as:

$$A = \begin{bmatrix} -1/\tau_1 & 0 & 0 & 0 \\ 0 & -1/\tau_2 & 0 & 0 \\ 0 & 0 & -1/\tau_3 & 0 \\ 0 & 0 & 0 & -1/\tau_4 \end{bmatrix},\ B_1 = \begin{bmatrix} 0 & 0 \\ 0 & 0 \\ 0 & 0 \\ 0 & 0 \end{bmatrix}$$

$$B_2 = \begin{bmatrix} 1/\tau_1 \\ 1/\tau_2 \\ 1/\tau_3 \\ 1/\tau_4 \end{bmatrix},\ C^{\mathrm{T}} = \begin{bmatrix} -1 \\ -1 \\ -1 \\ -1 \end{bmatrix},\ D_1 = [1 \quad -1],\ D_2 = 0$$

Corresponding input and output equations of the proposed system can be represented by a general notation as:

$$P = \left[\begin{array}{c|cc} A & B_1 & B_2 \\ \hline C & D_1 & D_2 \end{array}\right]$$

The H_∞ control problem is derived by reducing the norm of the closed loop transfer function of the linear fractional transformation (LFT) of $\tilde{T}_{\tilde{z}\tilde{w}}$ from $\tilde{w}$ to $\tilde{z}$. Where, $\tilde{w}$ and $\tilde{z}$ represent overall exogenous inputs and regulated outputs, respectively. The closed loop LFT and corresponding controller is represented by:

$$\begin{bmatrix} \tilde{z} \\ \tilde{y} \end{bmatrix} = \tilde{P} \begin{bmatrix} \tilde{w} \\ u \end{bmatrix},\ u = K * \tilde{y} \tag{16}$$

here, $\tilde{P}$ is aggregated plant that includes all parameters in Fig. 2 excluding controller, i,e., K. To obtain a sub-optimal solution of the LFT, norm of the closed loop system should be less than a constant value such that

$$\|\mathscr{F}(\tilde{P}, K)\|_\infty < \gamma \tag{17}$$

To present the proposed model according to (16), equations according to Fig. 2 are presented as:

$$\tilde{y} = e_{\mathrm{pcc}} + \zeta w_1 = \left[\begin{array}{c|cc} A & B_1 & B_2 \\ \hline C & D_1 & D_2 \end{array}\right] \begin{bmatrix} w \\ u \end{bmatrix} + \zeta w_1 \tag{18}$$

here, term w_1 is the noise in measurement of the error signal while ζ is the extra controlling parameter to vary the intensity of noise. For the application proposed in this study, the value of ζ is chosen to be 0.8 which shows that 80% of the noise signal is influencing the output error measurement. The overall output of the plant yields:

$$\tilde{y} = \left[\begin{array}{c|ccc} A & 0 & B_1 & B_2 \\ \hline C & \zeta & D_1 & D_2 \end{array}\right] \begin{bmatrix} w_1 \\ w \\ u \end{bmatrix} \tag{19}$$

Regulated outputs of the aggregated plant are given by:

$$z_1 = W_F * \tilde{y},\ z_2 = \sigma u \tag{20}$$

Constant σ is the extra parameter to restrict/enhance the effect of control signal. For the proposed model, the value of σ is chosen to be 2.5 which demonstrates an intense control signal application for the plant. In (20), W_F is the weighting function used to penalize DC values of error at PCC. Moreover, weighting function (W_F) is also used as a tool to further suppress fluctuations in error [32]. The general form of W_F is expressed as:

$$W_F = \left[\begin{array}{c|c} A_F & B_F \\ \hline C_F & D_F \end{array}\right] \tag{21}$$

here, terms A_F, B_F, C_F, and D_F are calculated through hit and trial method and the best values are chosen according to the optimum value of γ. The best values of the W_F are the ones at lowest obtained γ. The optimum values of A_F, B_F, C_F, and D_F are -0.65, 1, 0.675 , and 0.5, respectively. The aggregated output of the plant is the input to the weighting function (W_F). The regulated output including the filter yields:

$$z_1 = \left[\begin{array}{cc|ccc} A & 0 & 0 & B_1 & B_2 \\ B_F C & A_F & B_F\zeta & B_F D_1 & B_F D_2 \\ \hline D_F C & C_F & \zeta D_F & D_F D_1 & D_F D_2 \end{array}\right] \begin{bmatrix} w_1 \\ w \\ u \end{bmatrix} \tag{22}$$

After combining (18)–(22), the aggregated plant model can be concatenated as:

$$\tilde{P} = \left[\begin{array}{cc|ccc} A & 0 & 0 & B_1 & B_2 \\ B_F C & A_F & B_F\zeta & B_F D_1 & B_F D_2 \\ \hline D_F C & C_F & \zeta D_F & D_F D_1 & D_F D_2 \\ 0 & 0 & 0 & 0 & \sigma \\ C & 0 & \zeta & D_1 & D_2 \end{array}\right] \tag{23}$$

B. h_∞ Controller Derivation

At this point, the proposed concatenated plant model (23) can be used to derive H_∞ controller that minimizes H_∞-norm of closed-loop transfer function ($\tilde{T}_{\tilde{z}\tilde{w}}$) of the proposed system. In other words, the main motivation of the H_∞ controller synthesis is to propose a controller that minimizes influence of exogenous inputs ($\tilde{w}$) on regulated outputs ($\tilde{z}$) of the concatenated plant model [33]. Here, it is pertinent to mention that, the H_∞ control is a sub-optimal solution, therefore, the controller is designed in such a manner that the H_∞-norm of LFT of the concatenated plant model and the controller is less than predefined $\gamma = 2$. To find a sub-optimal H_∞ controller, the peak singular value across all frequencies should be less than the pre-defined value of γ. This scenario can be expressed by:

$$\|\mathscr{F}(\tilde{P}, K)\|_\infty = \max_{\omega} \overline{\sigma}(\mathscr{F}(\tilde{P}, K)(j\omega)) \tag{24}$$

For this agenda, MATLAB command hinfsyn is used to derive the required sub-optimal H_∞ controller. The hinfsyn command searches for a controller using the closed-loop system which has a peak singular value across all the frequencies. In other words, the hinfsyn command derives an H_∞ controller that minimizes the influence of exogenous inputs ($\tilde{w}$) and control input (u) on the plant while simultaneously regulating output ($\tilde{y}$) and regulated outputs ($\tilde{z}$) as expressed in (16). If the hinfsyn command returns a controller with a degree equal to the original plant model and the closed-loop gain is less than the pre-defined γ, then the closed-loop system is considered to be internally stable [34]. Using the hinfsyn command, the transfer function of the newly derived H_∞ controller is found to be of degree 5.

Using the newly extracted controller model, H_∞-norm of the designed closed-loop model is 1.70 which is less than the predefined limit of $\gamma = 2$. This analysis confirms that, the proposed controller meets design requirements of minimizing the norm of the closed-loop system and it makes the overall system internally stable [35]. The derived controller is strictly proper; however, such a high-order controller cannot be used for the proposed application. For this reason, nearby poles and zeros are canceled to reduce the order of the controller. The controller is reduced to:

$$K_{H_\infty} = \frac{32.827}{(s + 69.93)} \tag{25}$$

1) Rigidness Evaluation of the PCC

Sensitivity of parameters of PCC, followed by a disturbance, can be termed as rigidness of parameters. Since, the main motivation of the proposed H_∞ controller is to minimize the error between injected active and reactive power compared to demand reference communicated by the transmission system operator (TSO). Therefore, the H_∞ norm of the close-loop transfer function including the newly derived controller can provide sufficient information regarding the gain that describes rigidness of the PCC. The H_∞ norm including the original controller is 1.70. Similarly, the H_∞ norm of the closed-loop transfer function after including the reduced controller is 1.74. On the other hand, rigidness gain of the PCC for the conventional proportional controller as presented in [3] is above 6.6. This validates that the proposed controller highly minimizes the gain of the system and consequently improves rigidness of the PCC. Moreover, the above analysis also validates that, the performance of the reduced controller is almost similar to the original controller in terms of enhancing the rigidness of the PCC.

C. Eigenvalues Analysis

As established in the previous section, the closed-loop system is internally stable if there exists an H_∞ controller that successfully minimizes the norm of the closed-loop transfer function (17) to a smaller value (typically less than 2). However, the eigenvalue analysis is necessary to evaluate the convergence speed of the system to reach steady-state condition after a transient. Putting $u = K_{H_\infty} * \tilde{y}$ in (14) yields the closed-loop state model as:

$$\begin{aligned}\dot{x} = (A + B_2 K_{H_\infty} C)x + B_1 w + B_2 K_{H_\infty} D_1 w \\ + B_2 K_{H_\infty} \zeta w_1\end{aligned} \tag{26}$$

The above state model is used to calculate closed-loop norm of the designed system such that

$$\begin{aligned}\|T_{zw}\| = \|[D_1 D_2] + C(sI - (A + B_2 K_{H_\infty} C)^{-1})[B_1 B_2]\| \\ < \gamma\end{aligned} \tag{27}$$

Restricting the H_∞-norm of the closed-loop system less than pre-specified γ ensures minimum overshoot; however, this does not provide information regarding the transient phase time when the system is under the influence of disturbances. To analyze transient phase time, we introduce a virtual element in (14) such that

$$\dot{x}_{\text{New}} = (A + \delta I)x + B_1 w + B_2 \tag{28}$$

here, term δ is greater than zero and it is the supposed element that shows a shift in eigenvalues of the state matrix; and I is the identity matrix. With newly introduced δ, the new controller, i.e., $K_{H_{\infty}\text{New}}$, should also reduce the closed-loop norm such that

$$\begin{aligned}\|T_{zw\text{New}}\| = \|[D_1 D_2] + C(sI - (A + B_2 K_{H_\infty\text{New}} C \\ + \delta I)^{-1})[B_1 B_2]\| < \gamma_{\text{New}}\end{aligned} \tag{29}$$

At this point, if we consider the new controller ($K_{H_\infty\text{New}}$) for the original state model (14), it can be observed that $A + B_2 * K_{H_\infty\text{New}} C$ has all eigenvalues with real parts less than $-\delta$. From this analysis, it can be deduced that the new controller ensures that the convergent speed of the real system remains faster than $\mathrm{e}^{-\delta t}$.

It is pertinent to validate that, the H_∞-norm of the closed-loop system using the new controller ($K_{H_\infty\text{New}}$) is bounded by less than γ_{New}. The eigenvalues of the original plant ($\tilde{P}$) has the nearest eigenvalue to the origin at -0.4. If the newly introduced term (δ) is greater than 0.4, it will shift the nearest eigenvalue towards the right half plane. Therefore, only ($0 < \delta < 0.4$) will be considered for further analysis. The H_∞-norm after introducing δ using the plant ($\tilde{P}_\delta$) is calculated for different values of δ. At $\delta = 0.39$, H_∞ norm is calculated as 3 while the norm reduces up to 1.74 as δ is reduced to zero. On the contrary, if $\delta \geq 0.4$, the H_∞ norm reaches infinite value because the nearest eigenvalue shifts to right half plane. Using newly introduced δ and the newly derived controller ($K_{H_\infty\text{New}}$), the norm of the closed-loop system can be expressed as $\|T_{zw\text{New}}\|_\infty$ which is less than the norm of original system $\|T_{zw}\|_\infty$ (using the same ($K_{H_\infty\text{New}}$)) for $\delta < 0.4$. Satisfaction of (29) confirms that overshoot and transient phase time are satisfied. Moreover, for $\delta > 0.4$, the convergence speed of the system is too slow to retain its stable position after a disturbance. In other words, for an eigenvalue shift of $\delta < 0.4$, the closed-loop system will retain its convergence speed faster than $\mathrm{e}^{-\delta t}$.

IV. Numerical Simulation Results

The practicality of the proposed coordination control strategy is validated in MATLAB/SIMULINK software using the IEEE 13-bus test system provided in Fig. 1. The PCC of ADN is connected to a transmission line network (TLN) with 20 km line distance in order to weaken rigidness of PCC. Practically, longer distances increase line impedance hence weakening grid strength. Moreover, converter-interfaced IRESs are connected to high R/X ratio lines in order to realize a more realistic LV ADN. In addition, the reactive power capacity of each DG is chosen to be 32.25% of nominal active power capacity. It is obvious that, the maximum reactive power can only be supplied by DG when active power generation is less than nominal capacity, i.e., $Q_{\text{nom}} = 0.3225 * S_{\text{nom}}$ where $Q_{\text{nom}} = \sqrt{S_{\text{nom}} - P_{\text{DG}}}$. Further details of the proposed system are given in Table II.

Simulation starts with active power coordination activated at $t = 0$ s. Also, the PCC demand at the beginning is kept at -60 kW and -5 kVar. The negative sign shows that the ADN is feeding the grid. A constant power load of $P_{\text{L1}} = 50$ kW

TABLE II
SYSTEM PARAMETERS

Parameters	VSG1	VSG2	VSG3	VSG4
Active Power Capacity (kW)	60	50	65	75
Reactive Power Capacity (kVar)	19.35	16.125	20.96	24.1875
Moment of Inertia (J)	3.65	3.03	4.7466	5.3247
Damping Coefficient (D)	80	60	100	120
Active Power Droop Constant (K_p)	821.63e^{-5}	985.96e^{-5}	758.4042e^{-5}	657.3e^{-5}
Reactive Power Droop Constant (K_q)	1.6082e^{-3}	1.9299e^{-3}	1.4847e^{-3}	1.2866e^{-3}
LPF Time Constant, τ (s)	0.01	0.01	0.01	0.01
Reactive Power Inertia Constant, (K)	1/15	1/12	1/18	1/22
Virtual Resistance, (R_v)	0.1 Ω	0.1 Ω	0.1 Ω	0.1 Ω
Virtual Inductance, (L_v)	3 mH	3 mH	3 mH	3 mH
Feeder Line Impedance, Z_l	$0.20724 + \text{j}0.06908$	$0.41448 + \text{j}0.06908$	$0.27632 + \text{j}0.06908$	$0.3454 + \text{j}0.06908$
R/X ratio of feeder, (R_l/X_l)	3	6	4	5

& $Q_{\text{L1}} = 10$ kVar is attached to bus 1 and $P_{\text{L2}} = 40$ kW & $Q_{\text{L2}} = 10$ kVar is connected to bus 5 of the ADN. The PCC active power demand is increased to -90 kW at $t = 2$ s. At $t = 4$ s, the reactive power demand at PCC is changed to $+5$ kVar. At $t = 5.5$ s, reactive power coordination is activated. A plug and play load of $P_{\text{L3}} = 30$ kW & $Q_{\text{L3}} = 10$ kVar is attached to bus 1 of ADN at $t = 7$ s. To test rigidness of PCC against disturbances, a bulk load variation scenario is demonstrated in TLN at $t = 9$ s.

A. PCC Rigidness Enhancement

PCC is considered to be rigid if its parameters, such as voltage, active and reactive power, exhibit lower overshoots across the reference demand after a disturbance. For this reason, the aforementioned parameters are simulated to validate performance of the proposed strategy. Results of PQ management at PCC are given in Figs. 3–5. Moreover, to confirm the superiority of the proposed method, a comparison with conventional control, proposed in [3], is also provided in Figs. 3–5.

During start of simulation, it can be observed in Figs. 3–4 that, the active and reactive power at PCC using the proposed method allows lower overshoots as compared to the conventional method. A significant reduction in percentage overshoot is observed during initial transient at active power regulation. This confirms that the H_∞-norm reduction successfully minimizes overshoot during disturbances. In the beginning of simulation, reactive power regulation in Fig. 4 observed almost a similar peak in the conventional and the proposed method. However, after the first peak passed, the proposed method regulates the reactive power with smaller second peak as compared to the conventional method. Since, response of reactive power is related with voltage response, therefore, voltage (per unit) behavior in Fig. 5 shows a similar behavior in the beginning of simulation. However, the proposed method allows the system to reach steady state with lower peak oscillations. Voltage peaks at PCC in Fig. 5 validate that the proposed method enhances rigidness at PCC. To further test rigidness of the parameters, the active power demand at PCC is changed to -90 kW at $t = 2$ s and reactive power demand is changed to $+5$ kVar at $t = 4$ s. It can be observed in Figs. 3–5 that, the proposed method successfully fulfills the new active and reactive power demands with minimum peak overshoot. On the other hand, the conventional method experiences significant oscillations.

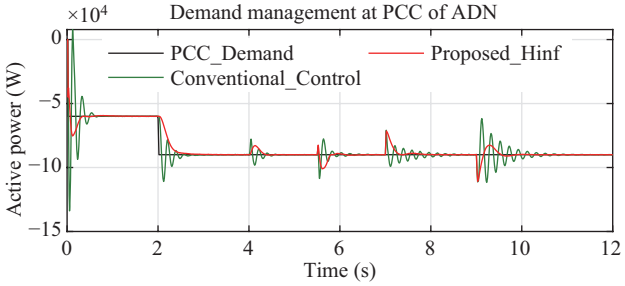

Fig. 3. Active power management at PCC of ADN.

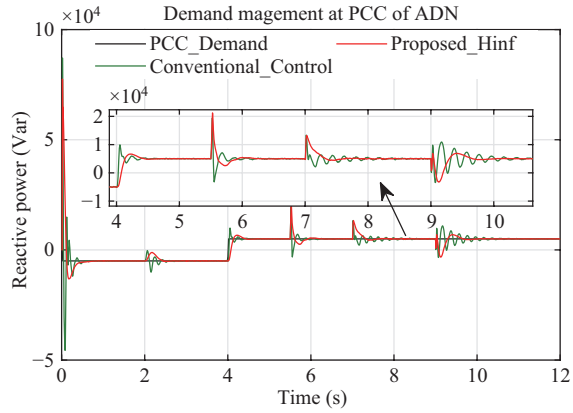

Fig. 4. Reactive power management at PCC of ADN.

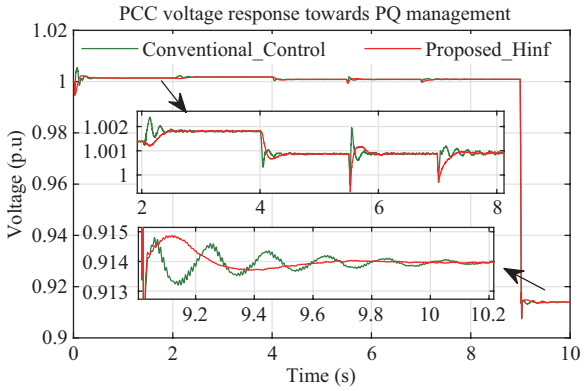

Fig. 5. Voltage assessment at PCC of ADN.

For analyzing the influence of disturbances within ADN, a plug and play load is attached at $t = 7$ s of the simulation. Figs. 3–5 shows that the proposed method outperforms the conventional method by mitigating peak oscillations inflicted by load variations. Moreover, unlike conventional method, there is no second peak emerging in the proposed method. Finally at $t = 9$ s, a disturbance in the TLN is inflicted to test its influence on the performance of PCC. In Figs. 3–5 it can be observed that, high peak oscillations experienced by the conventional method can be severely dangerous for the overall system equipment. It should be recalled that, due to coupling of PCC with the DGs through uni-directional broadcast communication, these oscillations will influence the power generation performance of the DGs as well as the sub-station transformer. It can be concluded from the results that, the proposed method successfully mitigates these oscillations. This analysis confirms that the proposed method offers higher damping against disturbances as compared to the conventional method. More importantly in practical scenarios, due to high penetration of IRESs, the substation transformer is already overwhelmed with unconsumed power which significantly raises voltage at PCC. For this reason, a rigid voltage at PCC is an essential feature for power systems with high penetration of IRESs.

B. Response of Multiple Operating Converters

In Figs. 6–7, the response of a distant DG (from the substation transformer) with lowest power rating is illustrated. Since, a distant DG has sensitive reactive power-voltage (Q-V) relation, therefore, comparing reactive power response of DG2 (which is lowest rating converter) can be more convenient in understanding the influence of the proposed method. Also, the main assessment here is based on maximum active and reactive power drawn by converters during disturbances. As power electronics converters have limited capacity, therefore, larger peaks can overload the converters and consequently damage switches of power electronics converters.

During initialization of the simulation, as obvious from Fig. 6, the converter using the proposed control scheme experiences a significantly lower overshoot as well as minimum oscillations as compared to the conventional method. This shows that enhancing the rigidness of parameters at PCC can also lead to better performance of power electronics converters. Moreover, lower oscillations and low amplitude peaks for reactive power response in Fig. 7 also validates the superior performance using the proposed control strategy.

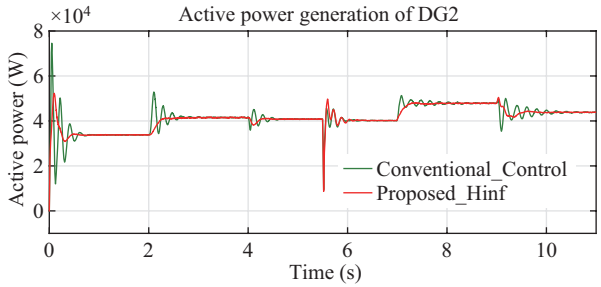

Fig. 6. Active power response assessment of DG2.

The same results also validate the superiority of the proposed method during disturbances such as PCC active power demand fluctuation at $t = 2$ s, PCC reactive power demand variation at $t = 4$ s, load demand variation at $t = 7$ s, and bulk load variation in TLN at $t = 9$ s.

In order to extend the analysis, results of the coordination between power electronics converters for the conventional method and the proposed H_∞ controller are also presented in Figs. 8 and 9. In these figures, the operation of tertiary control layer is shown where the convergence towards proportionate active and reactive power sharing is analyzed and compared for the conventional and proposed control strategy. Both strategies successfully converge to optimal coordination of all the power electronics converters; however, the proposed H_∞ controller is superior in reaching convergence with minimum oscillations after each disturbance. After each disturbance, in Fig. 8, active powers of all converters for the conventional control strategy experience huge oscillations before converging to proportionate active power sharing. These oscillations could practically overwhelm converters switches and lead to severe consequences for costly equipment. On the contrary, the proposed controller significantly suppresses active power oscillations. Moreover, reactive power coordination in Fig. 9 also shows that the proposed strategy offers fewer oscillations while converging to proportional reactive power generation.

C. Influence on the Performance of Frequency

The influence of the proposed strategy on the performance

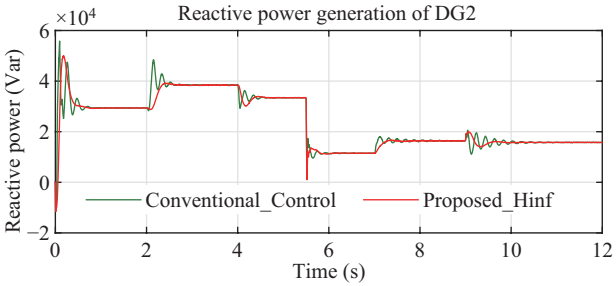

Fig. 7. Reactive power response assessment of DG2.

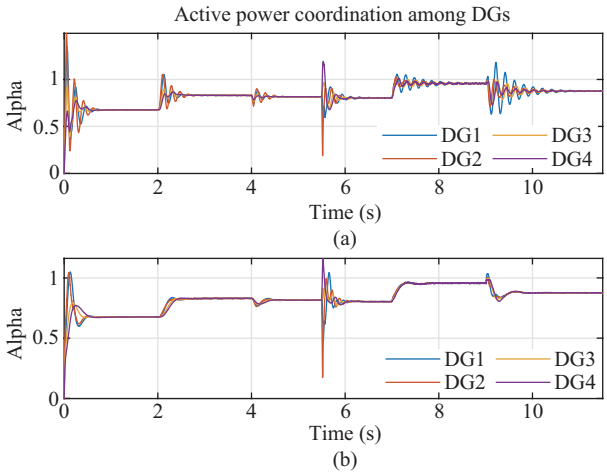

Fig. 8. Active power coordination index. (a) Conventional method. (b) Proposed H_∞ method.

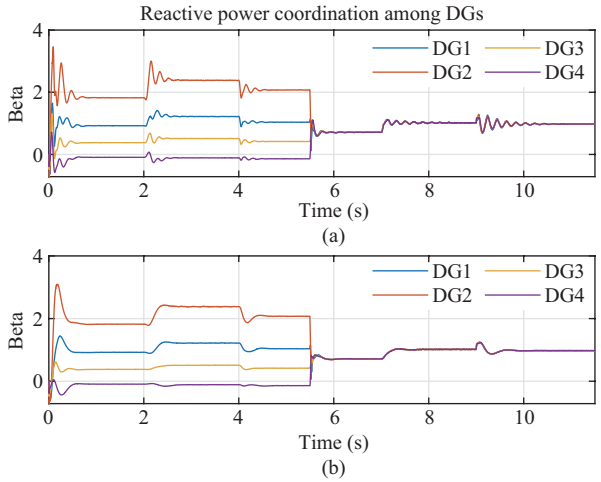

Fig. 9. Reactive power coordination index. (a) Conventional method. (b) Proposed H_∞ method.

of frequency of the system is illustrated in Fig. 10. As evident from Fig. 10 at $t = 2$ s, 4 s, 5.5 s, 7 s, and 9 s, the proposed H_∞ control offers rigid frequency performance towards demand fluctuation at PCC as compared to the conventional method. For any disturbance, the frequency in conventional method experiences greater peak amplitudes which are highly suppressed by the proposed control strategy. Especially, a significant difference can be observed when the PCC demand is abruptly changed at $t = 2$ s and 4 s. At this time, the conventional control strategy experiences significant oscillations in frequency. While for the same amount of demand fluctuation, the proposed H_∞ control strategy significantly suppresses oscillations. At $t = 7$ s, a plug and play load of $P_{L3} = 30$ kW & $Q_{L3} = 10$ kVar is attached near the PCC. At this point, the conventional control experiences slightly higher peaks of oscillations as compared to the proposed proposed H_∞ control strategy. However, this difference will be stretched if the load demand varies in greater magnitude. For instance, at $t = 9$ s, a load variation of high amplitude is demonstrated in the TLN which causes frequency oscillations of high amplitude for the conventional control strategy. However, in Fig. 10, rigid active power management at PCC offered by the proposed H_∞ controller timely suppresses frequency oscillations. The above analysis clearly shows that the proposed strategy significantly overcomes the shortcomings of the conventional control strategy.

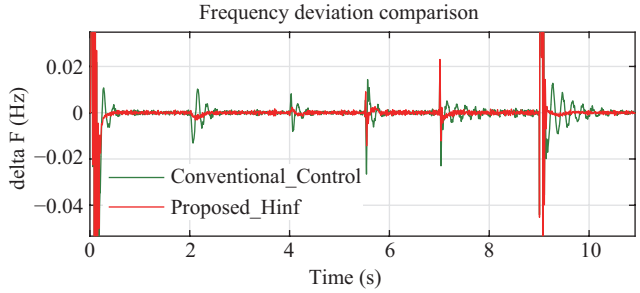

Fig. 10. Effect of fluctuations at PCC on the frequency deviation.

D. Testing the Scalability of the Proposed Method

To further validate its practicality, the proposed method is implemented on an IEEE 34-bus test system given in Fig. 11. In this figure, nodes in green show idle buses while nodes in blue represent points where DGs are connected. The communication link for bi-directional information exchange is represented as light blue lines while uni-directional broadcast communication is represented by red lines. Further details of the IEEE 34-bus system are given in [29]. Results of the proposed method are given in Figs. 12–14. In Fig. 12, active and reactive power management is smoothly handled using the proposed method as evidence by the response towards disturbances at $t = 2$ s, and 3 s. In conclusion, implementing the proposed method on a large scale system validates scalability of the proposed method however, the location of DGs according to its size is a matter of optimal power flow study.

By expanding the scale of the system, the impact of information delay (due to longer communication lines) cannot be ignored. With expansion of the size of the system

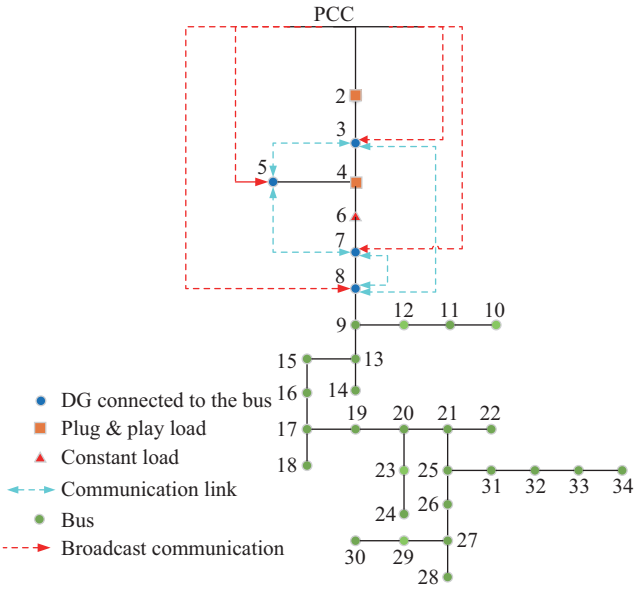

Fig. 11. IEEE 34-bus test distribution system [29].

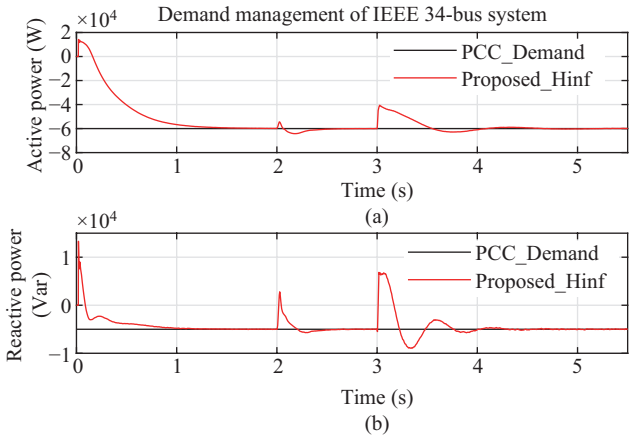

Fig. 12. Demand management at PCC using IEEE34-bus test system. (a) Active power management. (b) Reactive power management.

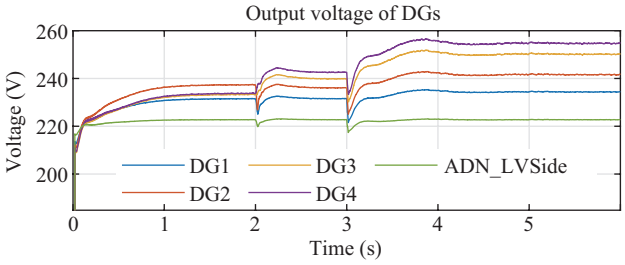

Fig. 13. Output voltages of DGs.

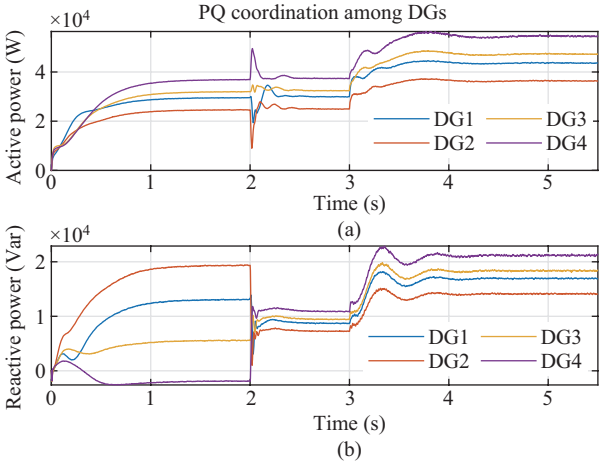

Fig. 14. PQ coordination among DGs. (a) Active power generation of DGs. (b) Reactive power generation of DGs.

communication delays or data packet loss will hinder the performance of broadcast information. However, as reported by [36], combination of wired and wireless broadcast communication infrastructure can fulfill PCC deviation communication requirements for a network of hundreds of DGs which is enough for application of ADN. Therefore, the proposed strategy is tested by introducing a communication delay at premises of each DG. Since, the PCC demand management is fulfilled by response of DGs, therefore, delay in the arrival of reference can inflict a realistic scenario. In active power broadcast, a delay of 0.1 s, 0.13 s, 0.16 s and 0.19 s is introduced at DG1, DG2, DG3, and DG4, respectively. The effect of these delays can be witnessed in Fig. 14(a) at $t = 3$ s. The proposed method experiences slight oscillations, however, active power generations converge to steady-state condition. Similarly, for reactive power broadcast, a delay of 0.1 s, 0.05 s, 0.05 s and 0.05 s is introduced at DG1, DG2, DG3, and DG4, respectively. Here, delay introduces oscillations due to the direct relation of voltage and reactive power generation. Hence, until reactive power reaches steady state condition, voltage at the nearby PCC will keep oscillating. For this reason, delay in reactive power broadcast is kept small to lower the impact on the voltage profile of the nearby PCC of each DG. It is understandable that, longer delays in reactive power reference broadcast can severely degrade the voltage profile at the nearby nodes. The shortcoming of voltage collapse due to longer delays is a matter of future research. Moreover, installation of DGs at a longer distance may increase line impedance between local PCC of the respective DG and the substation transformer. Such situation increases reactive power to voltage sensitivity of the DG as shown in Fig. 13. Compared to a DG located near the substation, the DG located far from the substation will generate/absorb more reactive power for a voltage variation. This situation is a matter of optimal allocation and sizing of DGs rather than an issue in scalability of the proposed control strategy. For optimal sizing and allocation of DGs, several optimization methods are reported in [37]. This analysis concludes the proposed method is flexible towards scalability, overcomes severe delay issues in active power broadcast signals, and minor delay issues in reactive power broadcast signals.

V. Conclusion

This study has presented a new perspective for analyzing rigidness of parameters of high voltage PCC of an ADN. A complete aggregated plant model is derived that includes the exogenous inputs and regulated outputs. Moreover, an H_∞ controller is derived to reduce the H_∞-norm of the closed loop system. This analysis have led the quantification of the gain of the rigidness of PCC. The proposed method is tested on a generic IEEE 13-bus test system and IEEE 34-bus distribution system. Also, results have confirmed that using the proposed method, the enhancement of rigidness of the PCC also improves the performance of frequency of the system and convergence response of active and reactive power from coordinated converter-interfaced DGs. Furthermore, an eigenvalue analysis was also presented that elaborated the convergence speed situation of the closed-loop model. Finally, the obtained results confirmed the superiority of the proposed method in terms of suppressing overshoot of active and reactive power management at high voltage PCC, as well as local power regulation of each DG.

References

[1] N. C. Koutsoukis, P. S. Georgilakis, and N. D. Hatziargyriou, "Multistage coordinated planning of active distribution networks," *IEEE Transactions on Power Systems*, vol. 33, no. 1, pp. 32–44, Jan. 2018.

[2] Z. Q. Yang, Y. J. Li, and J. Xiang, "Coordination control strategy for power management of active distribution networks," *IEEE Transactions on Smart Grid*, vol. 10, no. 5, pp. 5524–5535, Sep. 2019.

[3] S. Fahad, A. Goudarzi, and J. Xiang, "Demand management of active distribution network using coordination of virtual synchronous generators," *IEEE Transactions on Sustainable Energy*, vol. 12, no. 1, pp. 250–261, Jan. 2021.

[4] G. Mokhtari, G. Nourbakhsh, and A. Ghosh, "Smart coordination of energy storage units (ESUs) for voltage and loading management in distribution networks," *IEEE Transactions on Power Systems*, vol. 28, no. 4, pp. 4812–4820, Nov. 2013.

[5] K. T. Tan, P. L. So, Y. C. Chu, and M. Z. Q. Chen, "Coordinated control and energy management of distributed generation inverters in a microgrid," *IEEE Transactions on Power Delivery*, vol. 28, no. 2, pp. 704–713, Apr. 2013.

[6] H. Beltran, E. Bilbao, E. Belenguer, I. Etxeberria-Otadui, and P. Rodriguez, "Evaluation of storage energy requirements for constant production in PV power plants," *IEEE Transactions on Industrial Electronics*, vol. 60, no. 3, pp. 1225–1234, Mar. 2013.

[7] H. H. Xin, M. D. Zhang, J. Seuss, Z. Wang, and D. Q. Gan, "A real-time power allocation algorithm and its communication optimization for geographically dispersed energy storage systems," *IEEE Transactions on Power Systems*, vol. 28, no. 4, pp. 4732–4741, Nov. 2013.

[8] N. Jabalameli, M. A. S. Masoum, F. Shahnia, and T. H. Mehr, "Impact of battery rating on performance of rooftop PV supporting household loads, regulating PCC voltage and providing constant output power to grid," in *2013 Australasian Universities Power Engineering Conference (AUPEC)*, Hobart, TAS, Australia, 2013, pp.1–6.

[9] Y. Mishra, S. Mishra, and F. X. Li, "Coordinated tuning of DFIG-based wind turbines and batteries using bacteria foraging technique for maintaining constant grid power output," *IEEE Systems Journal*, vol. 6, no. 1, pp. 16–26, Mar. 2012.

[10] D. Wang, S. Y. Ge, H. J. Jia, C. S. Wang, Y. Zhou, N. Lu, and X. Y. Kong, "A demand response and battery storage coordination algorithm for providing microgrid tie-line smoothing services," *IEEE Transactions on Sustainable Energy*, vol. 5, no. 2, pp. 476–486, Apr. 2014.

[11] D. E. Olivares, A. Mehrizi-Sani, A. H. Etemadi, C. A. Cañizares, R. Iravani, M. Kazerani, A. H. Hajimiragha, O. Gomis-Bellmunt, M. Saeedifard, R. Palma-Behnke, G. A. Jiménez-Estévez, and N. D. Hatziargyriou, "Trends in microgrid control," *IEEE Transactions on Smart Grid*, vol. 5, no. 4, pp. 1905–1919, Jul. 2014.

[12] N. R. Tummuru, M. K. Mishra, and S. Srinivas, "Dynamic energy management of renewable grid integrated hybrid energy storage system," *IEEE Transactions on Industrial Electronics*, vol. 62, no. 12, pp. 7728–7737, Dec. 2015.

[13] G. Chen, F. L. Lewis, E. N. Feng, and Y. D. Song, "Distributed optimal active power control of multiple generation systems," *IEEE Transactions on Industrial Electronics*, vol. 62, no. 11, pp. 7079–7090, Nov. 2015.

[14] Y. L. Xu and Z. C. Li, "Distributed optimal resource management based on the consensus algorithm in a microgrid," *IEEE Transactions on Industrial Electronics*, vol. 62, no. 4, pp. 2584–2592, Apr. 2015.

[15] W. Zhang, Y. Ma, W. X. Liu, S. J. Ranade, and Y. S. Luo, "Distributed optimal active power dispatch under constraints for smart grids," *IEEE Transactions on Industrial Electronics*, vol. 64, no. 6, pp. 5084–5094, Jun. 2017.

[16] T. Q. Zhao and Z. T. Ding, "Distributed finite-time optimal resource management for microgrids based on multi-agent framework," *IEEE Transactions on Industrial Electronics*, vol. 65, no. 8, pp. 6571–6580, Aug. 2018.

[17] H. Pourbabak, J. W. Luo, T. Chen, and W. C. Su, "A novel consensus-based distributed algorithm for economic dispatch based on local estimation of power mismatch," *IEEE Transactions on Smart Grid*, vol. 9, no. 6, pp. 5930–5942, Nov. 2018.

[18] H. H. Xin, Z. H. Qu, J. Seuss, and A. Maknouninejad, "A self-organizing strategy for power flow control of photovoltaic generators in a distribution network," *IEEE Transactions on Power Systems*, vol. 26, no. 3, pp. 1462–1473, Aug. 2011.

[19] H. H. Xin, Z. Qu, Z. H. Lu, D. F. Gan, and D. Qi, "Cooperative control strategy for multiple photovoltaic generators in distribution networks," *IET Control Theory & Applications*, vol. 5, no. 14, pp. 1617–1629, Sep. 2011.

[20] X. W. Yan, A. Rasool, F. Abbas, H. Rasool, and H. X. Guo, "Analysis and optimization of the coordinated multi-VSG sources," *Electronics*, vol. 8, no. 1, pp. 28, Dec. 2018.

[21] P. Hu, H. K. Chen, K. Cao, Y. C. Hu, D. Kai, L. Chen, and Y. Wang, "Coordinated control of multiple virtual synchronous generators in mitigating power oscillation," *Energies*, vol. 11, no. 10, pp. 2788, Oct. 2018.

[22] Y. Hirase, O. Noro, H. Nakagawa, E. Yoshimura, S. Katsura, K. Abe, K. Sugimoto, and K. Sakimoto, "Decentralised and interlink-less power interchange among residences in microgrids using virtual synchronous generator control," *Applied Energy*, vol. 228, pp. 2437–2447, Oct. 2018.

[23] G. Yao, Z. C. Lu, Y. D. Wang, M. Benbouzid, and L. Moreau, "A virtual synchronous generator based hierarchical control scheme of distributed generation systems," *Energies*, vol. 10, no. 12, pp. 2049, Dec. 2017.

[24] S. Fahad, A. Goudarzi, and J. Xiang, "From grid feeding to grid supporting converters: A constant power active distribution network perspective," in *2020 IEEE 29th International Symposium on Industrial Electronics (ISIE)*, Delft, Netherlands, Jun. 2020, pp. 862–867.

[25] L. X. Meng, A. Luna, E. R. Díaz, B. Sun, T. Dragicevic, M. Savaghebi, J. C. Vasquez, J. M. Guerrero, and M. Graells, "Flexible system integration and advanced hierarchical control architectures in the microgrid research laboratory of aalborg university," *IEEE Transactions on Industry Applications*, vol. 52, no. 2, pp. 1736–1749, Mar./Apr. 2016.

[26] F. Bandeiras, E. Pinheiro, M. Gomes, P. Coelho, and J. Fernandes, "Review of the cooperation and operation of microgrid clusters," *Renewable and Sustainable Energy Reviews*, vol. 133, pp. 110311, Nov. 2020.

[27] H. R. Baghaee, M. Mirsalim, and G. B. Gharehpetian, "Performance improvement of multi-DER microgrid for small- and large-signal disturbances and nonlinear loads: Novel complementary control loop and fuzzy controller in a hierarchical droop-based control scheme," *IEEE Systems Journal*, vol. 12, no. 1, pp. 444–451, Mar. 2018.

[28] L. X. Meng, E. R. Sanseverino, A. Luna, T. Dragicevic, J. C. Vasquez, and J. M. Guerrero, "Microgrid supervisory controllers and energy management systems: A literature review," *Renewable and Sustainable Energy Reviews*, vol. 60, pp. 1263–1273, Jul. 2016.

[29] K. P. Schneider, B. A. Mather, B. C. Pal, C. W. Ten, G. J. Shirek, H. Zhu, J. C. Fuller, J. L. R. Pereira, L. F. Ochoa, L. R. De Araujo, R. C. Dugan, S. Matthias, S. Paudyal, T. E. McDermott, and W. Kersting, "Analytic considerations and design basis for the IEEE distribution test feeders," *IEEE Transactions on Power Systems*, vol. 33, no. 3, pp. 3181–3188, May 2018.

[30] S. Fahad, A. Goudarzi, Y. J. Li, and J. Xiang, "A coordination control strategy for power quality enhancement of an active distribution network," *Energy Reports*, vol. 8, no. 1, pp. 5455–5471, Nov. 2022.

[31] S. Cafieri, P. Hansen, and L. Liberti, "Loops and multiple edges in modularity maximization of networks," *Physical Review E*, vol. 81, no. 4, pp. 046102, Apr. 2010.

[32] S. D. Tavakoli, S. Fekriasl, E. Prieto-Araujo, J. Beerten, and O. Gomis-Bellmunt, "Optimal H_∞ control design for MMC-based HVDC links," *IEEE Transactions on Power Delivery*, vol. 37, no. 2, pp. 786–797, Apr. 2022.

[33] Q. C. Zhong, *Robust Control of Time-delay Systems*. London: Springer, 2006.

[34] P. Skogestad and I. Postlethwaite, *Multivariable Feedback Control: Analysis and Design*, 2nd ed., New York: John Wiley and Sons, 2005.

[35] H. Bevrani, *Robust Power System Frequency Control*. New York: Springer, 2014.

[36] S. Abadal, A. Mestres, M. Nemirovsky, H. Lee, A. González, E. Alarcón, and A. Cabellos-Aparicio, "Scalability of broadcast performance in wireless network-on-chip," *IEEE Transactions on Parallel and Distributed Systems*, vol. 27, no. 12, pp. 3631–3645, Dec. 2016.

[37] W. S. Tan, M. Y. Hassan, M. S. Majid, and H. A. Rahman, "Optimal distributed renewable generation planning: A review of different approaches," *Renewable and Sustainable Energy Reviews*, vol. 18, pp. 626–645, Feb. 2013.

Shah Fahad received B.S. degree in Electrical (power) Engineering from COMSATS University, Abbottabad, Pakistan, in 2015, and the M.S. degree in Electrical Power and Control from the CECOS University of IT and Emerging Sciences, Peshawar, Pakistan, in 2018. In 2022, he completed the Ph.D. degree in Electrical Engineering with the College of Electrical Engineering, Zhejiang University, Hangzhou, China. From 2022 to 2024, he has been working as a postdoctoral research scholar at the Missouri University of Science and Technology, Rolla, MO, USA. Currently, he is working as a Senior Power Systems Engineer at ETAP, Irvine, CA, USA. In 2018, Dr. Fahad won a fully-funded scholarship from the CSC to support his Ph.D. studies. He is an active researcher with several research publications in SCI indexed journals and international conference proceedings. He has served as a reviewer for several international journals that include IEEE Transactions on Sustainable Energy, IEEE Transactions on Power Systems, IEEE Transactions on Consumer Electronics, and Applied Energy. In March 2022, he was selected for a fully funded visiting researcher position in Qatar University. In March 2022, he was invited for a talk on impacts of high penetration levels of RESs on power systems arranged by IEEE Qatar section, Qatar university. His research interests include coordination control of converter-interfaced distributed generators, hierarchical control of microgrids, robust control, and applications of artificial intelligence/machine learning aided control techniques in RESs based power systems.

Arman Goudarzi received the B.Sc. degree from IAUB, Booshehr, Iran, in 2004 and the M.Sc. and Ph.D. degrees from the Mapua University and the University of KwaZulu-Natal, in the Philippines and South Africa in 2012 and 2017, respectively, all in Electrical Engineering. In 2018, he was selected as an international talent by the Chinese government under the talent introduction program during his course of extensive research as a postdoctoral fellow at Zhejiang University, China. He is currently working as an EV charging and infrastructure, Co-Op at General Motors (GM) Canada. He has served as a reviewer for various international journals and conferences; during this time, he acted as a scientific committee member of ICCE 2020 and 2021 in Ottawa, Canada, ICREN 2020 in Rome, Italy, and EEES 2023 in Dali, China. His main research interests include IoT-enabled smart grids, demand response (DR), EV charging, infrastructure and integration, electricity markets, GHGs reduction, and AI & machine learning applications in electrical engineering.

Pierluigi Siano received the M.Sc. degree in Electronic Engineering and the Ph.D. degree in Information and Electrical Engineering from the University of Salerno, Salerno, Italy, in 2001 and 2006, respectively. He is a Professor and Scientific Director of the Smart Grids and Smart Cities Laboratory with the Department of Management & Innovation Systems, University of Salerno. Since 2021 he has been a Distinguished Visiting Professor in the Department of Electrical & Electronic Engineering Science, University of Johannesburg. His research activities are centered on demand response, energy management, the integration of distributed energy resources in smart grids, electricity markets, and planning and management of power systems. In these research fields, he has co-authored more than 700 articles including more than 410 international journals that received in Scopus more than 16200 citations with an H-index equal to 62. In the period 2019-2022 he has been awarded as a Highly Cited Researcher in Engineering by Web of Science Group. He has been the Chair of the IES TC on Smart Grids. He is Editor for the Power & Energy Society Section of IEEE Access, IEEE Transactions on Power Systems, IEEE Transactions on Industrial Informatics, IEEE Transactions on Industrial Electronics, IEEE Systems.

Ji Xiang received the B.S degree from North China University of Technology, Beijing, China, in 1996. He received his M.S. and Ph.D. degrees from Zhejiang University, Hangzhou, China, in 1999 and 2005 respectively. From 2005 to 2007, he worked as a Postdoctoral Researcher in Zhejiang University and visited City University of Hong Kong for three months. Under the support of a Gleddens Senior Visiting Fellowship, he visited the University of Western Australia in 2008. During the year of 2013, he visited the University of Sydney as a visiting scholar. His research interests include networked dynamic systems, microgrids and underwater vehicles. Dr. Xiang is a Senior Member of the IEEE Control Systems Society. He is currently a Professor with the Department of System Science and Engineering at Zhejiang University.